Available online at www.sciencedirect.com

ScienceDirect

Journal of the European Ceramic Society 31 (2011) 2641–2648

www.elsevier.com/locate/jeurceramsoc

# Superplastic deformation of hydroxyapatite ceramics with $B_2O_3$ or $Na_2O$ addition fabricated by pulse current pressure sintering

Kiyoshi Itatani[a,*], Kenta Tsuchiya[a], Yoshio Sakka[b], Ian J. Davies[c], Seiichiro Koda[a]

[a] Sophia University, Department of Materials and Life Sciences, 7-1 Kioi-cho, Chiyoda-ku, Tokyo, Japan
[b] National Institute for Materials Science, Fine Particle Processing Group, 1-2-1 Sengen Tsukuba, Ibaragi, Japan
[c] Curtin University, Department of Mechanical Engineering, GPO Box U1987, Perth, Australia

## Abstract

High-density and fine-grained transparent hydroxyapatite ($Ca_{10}(PO_4)_6(OH)_2$: HAp) ceramics with $B_2O_3$ and $Na_2O$ addition were fabricated using pressureless sintering and pulse-current pressure sintering between 1000 and 1100 °C; the superplastic deformation of these HAp specimens was evaluated. The relative density of pure HAp compacts pulse-current pressure sintered at 1000 °C for 10 min under a pressure of 50 MPa attained 99.9% and exhibited translucency. The tensile elongation of the pure HAp specimen, which was measured at 1000 °C under a strain rate of $1.48 \times 10^{-4}\ s^{-1}$, was as high as 364%. The relative density of HAp compacts with 3.0 mol.% $B_2O_3$ addition pulse-current pressure sintered under the same conditions as those of pure HAp compacts was 98.9%, whereas the grain size was as low as 0.24 μm. The elongation of HAp specimens, measured at a test temperature of 1000 °C under a strain rate of $1.48 \times 10^{-4}\ s^{-1}$, was as high as 578%.

*Keywords:* Sintering; Grain size; Superplasticity; Apatite; Pulse current pressure sintering

## 1. Introduction

Hydroxyapatite ($Ca_{10}(PO_4)_6(OH)_2$; HAp) possesses a chemical composition comparable to the inorganic component of human bones and has been used in various forms of biomaterials (powder, granules, dense/porous bodies, etc.) due to its excellent biological compatibility within living tissue.[1,2] The dense form of HAp has found application as space filler material for bioactive fixation, whereas the porous form is currently used as a bone substitute for biological fixation. The dense form of HAp is also known to exhibit superplasticity, *i.e.*, deformation of polycrystalline material at elevated temperature, due to grain boundary sliding. The enhancement of grain boundary sliding may be achieved by controlling the density, grain size (usually <1 μm) and strain rate.[3,4] Owing to the optimization of these parameters, one of the present authors has succeeded in achieving tensile elongations of approximately 550% for alumina ($Al_2O_3$)–10 vol.% zirconia ($ZrO_2$),[5] 1000% for 0.3 vol.% $Al_2O_3$ dispersed tetragonal $ZrO_2$[6] and 2500% for $40ZrO_2(3Y)–30MgAl_2O_4–Al_2O_3$.[7] The superplasticity of HAp has previously been noted by Wakai et al.[8] who reported that the tensile strain of HAp specimens fabricated by hot isostatic pressing attained 153%, but that the tensile strain of HAp specimens fabricated by pressureless sintering was limited to 35%. More recently, the present authors have fabricated dense HAp specimens by pressureless sintering and found that the elongation at 1100 °C attained 157%.[9] Furthermore, a two-step pressureless sintering technique was applied to HAp compacts, *i.e.*, (i) heating of the compact to a temperature ($T_1$) where sintering initiates in the intermediate stage, (ii) cooling to a temperature ($T_2$: $T_1 > T_2$), (iii) holding for the desired time, and then (iv) cooling to room temperature. Owing to the utilization of this technique, the tensile elongation of HAp specimens was further increased to 188%—this was attributed to the grain size of the resulting HAp specimens being restricted to 0.44 μm, regardless of the high density (=98.8%).[10]

As noted above, the presence of relatively small grain sizes, in addition to high density, may be a key factor for the noted elongation of HAp ceramic materials. Moreover, grain boundary modification seems to be needed in order to accelerate the

---

[*] Corresponding author at: Department of Materials and Life Sciences, Faculty of Science and Engineering, Sophia University, 7-1 Kioi-cho, Chiyoda-ku, Tokyo 102-8554, Japan. Tel.: +81 3 3238 3373; fax: +81 3 3238 3361.
*E-mail address:* itatani@sophia.ac.jp (K. Itatani).

0955-2219/$ – see front matter © 2011 Elsevier Ltd. All rights reserved.
doi:10.1016/j.jeurceramsoc.2011.01.014

sliding of grains, which may also contribute to the superplastic deformation of HAp ceramic materials. In order to modify the properties of the grain boundary, the present authors[11] have considered the possibility of utilizing compounds in the $Na_2O$ and $B_2O_3$ system on the basis that fused materials formed at comparatively low temperature[12] may contribute to accelerating densification, and that the vitreous phase formed on the grain boundary during fabrication may assist grain sliding.

On the basis of such information, the present paper describes (i) conditions for the fabrication of high-density and fine-grained HAp ceramics with $Na_2O$ and/or $B_2O_3$ addition utilizing pressureless sintering and pulse current pressure sintering, and (ii) evaluation of superplastic deformation for these ceramic materials.

## 2. Experimental procedure

### 2.1. Fabrication of dense HAp ceramics with $Na_2O$ and $B_2O_3$ addition

A commercially available reagent grade HAp (HAp-100; Taihei-Kagaku Sangyo, Osaka), $Na_2CO_3$ (Wako Pure Chemical Ind., Tokyo, Japan) and $B_2O_3$ (Nakalai Tesque, Kyoto) were used as starting materials. The HAp powder was mixed with 1–10 mol.% $Na_2CO_3$ and $B_2O_3$ powders using ball-milling. Note that $Na_2CO_3$, instead of $Na_2O$, was incorporated into the starting HAp powder, due to the fact that $Na_2O$ is very sensitive to the presence of moisture in air. Cylindrical compacts with a diameter of 20 mm and a thickness of approximately 3 mm were fabricated by uniaxially pressing approximately 2 g of the powder at 50 MPa, followed by pressureless sintering. Similarly, cylindrical compacts with a diameter of 30 mm and a thickness of approximately 3 mm were fabricated by uniaxially pressing approximately 12 g of the powder at 50 MPa, followed by pulse-current pressure sintering (PCPS; SPS-1050, Sumitomo Coal Mining Co., Tokyo) under a pressure of 50 MPa. The heating rate from room temperature to the desired temperature was 25 °C $min^{-1}$.

### 2.2. Evaluation

Phase identification was carried out using an X-ray diffractometer (XRD: RINT 2000 V/P, Rigaku Corp., Tokyo, 40 kV and 40 mA) with monochromatic CuKα radiation; phases present at elevated temperature were examined using a high-temperature XRD equipped with an electric furnace. The expansion-shrinkage of powder compacts was examined using a thermo-mechanical analyzer (TMA; Model TAS-100, Rigaku, Tokyo) at a heating rate of 10 °C $min^{-1}$; cylindrical compacts with a diameter of 5 mm and a thickness of 3 mm were fabricated by uniaxially pressing approximately 0.1 g of the powder at 50 MPa, followed by cold-isostatically pressing at 100 MPa. The relative density of the sintered compacts was calculated on the basis of bulk density and theoretical density (=3.16 g $cm^{-3}$) with the bulk density being measured by the Archimedes method, using ethanol as a replacement liquid. The microstructure of sintered compacts was observed using a scanning electron microscope (SEM; Model S-4500, Hitachi, Tokyo, Japan) with an accelerating voltage of 5 kV. On the basis of SEM micrographs, the grain sizes were determined as $\pi/2$ times the linear intercept length.

Tensile tests of the resulting specimens were conducted in air at a temperature between 1000 and 1100 °C under a strain rate of $1.49 \times 10^{-5}\ s^{-1}$ and gauge length of 9 mm on a universal testing machine (TENSILON-1310, A&D Company, Tokyo, Japan) equipped with an infrared furnace. The true tensile stress–strain relationship was calculated by assuming that uniform linear deformation occurred during elongation; the true stress was calculated from the initial cross-section and resulting strain.

## 3. Results and discussion

### 3.1. Properties of HAp compacts with $Na_2O$ or $B_2O_3$ addition fabricated by pressureless sintering

Prior to checking the relative densities of HAp ceramics with $Na_2O$ or $B_2O_3$ addition, the thermal expansion-shrinkage behavior of the compacts was examined using TMA with the results being presented in Fig. 1. The shrinkage of the pure HAp compact started at approximately 700 °C and increased with temperature; the majority of the densification being completed by 1000 °C (Fig. 1(a)). In contrast to this, shrinkage of the HAp compact with 3.0 mol.% $Na_2O$ addition started to occur at approximately 700 °C, and slightly increased with temperature from 700 to 950 °C when compared to the case of the pure HAp compact (Fig. 1(b)). On the other hand, complete shrinkage of the HAp compact with 3.0 mol.% $B_2O_3$ addition was delayed until the temperature reached 1200 °C (Fig. 1(c)).

As the above results indicate, the shrinkage of HAp compacts may be promoted by the addition of $Na_2O$ (temperature range: 700–950 °C) but may be delayed by the addition of $B_2O_3$.

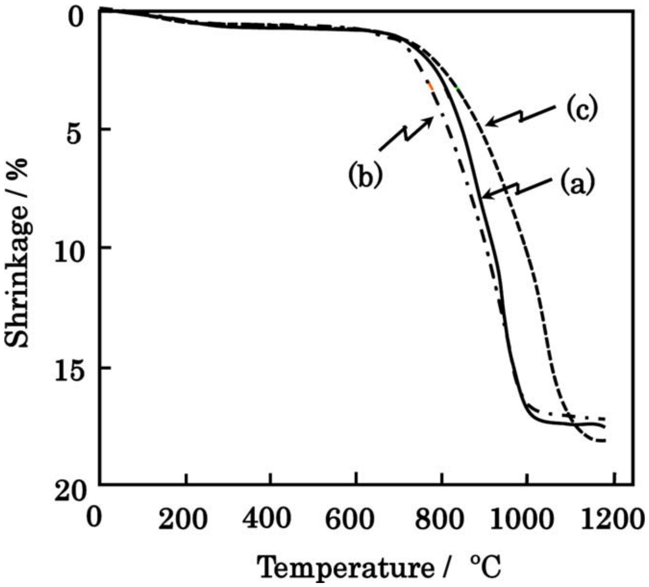

Fig. 1. Shrinkage behavior of (a) HAp compact, (b) HAp compact with 3.0 mol.% $Na_2O$ addition and (c) HAp compact with 3.0 mol.% $B_2O_3$ addition, at a heating rate of 10 °C $min^{-1}$.

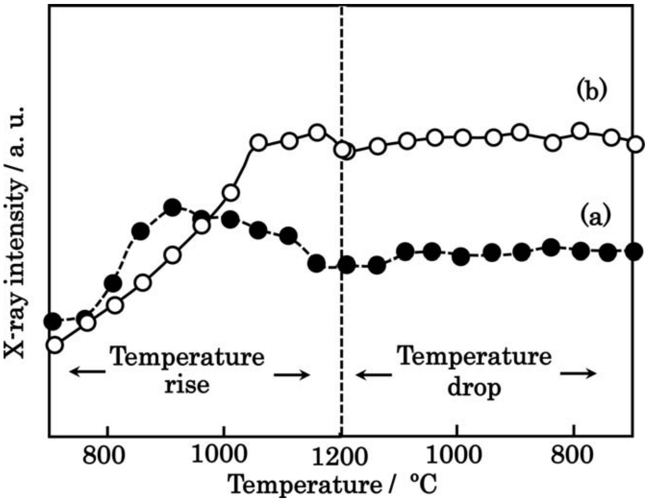

Fig. 2. Changes in X-ray intensity (3 0 0) ($2\theta = 32.8°$) for HAp powder with (a) 10 mol.% $Na_2O$ addition and (b) 10 mol.% $B_2O_3$ addition during heating and cooling at a rate of 10 °C $min^{-1}$.

In order to make clear such densification behavior, the reaction processes of HAp with $Na_2O$ and $B_2O_3$ were examined using high-temperature X-ray diffraction. Note that the amount of $Na_2O$ or $B_2O_3$ was increased from 3.0 to 10 mol.% in order to clearly understand the reaction process. Fig. 2 shows the changes in diffraction intensity of the (3 0 0) peak for HAp powder containing 10 mol.% $Na_2CO_3$ or $B_2O_3$ upon heating and cooling. When 10 mol.% of $Na_2O$ was incorporated into HAp powder, the diffraction intensity of HAp increased with increasing temperature to 900 °C but decreased with a further increase in temperature to 1200 °C; the diffraction intensity of HAp remained unchanged during the cooling process to 700 °C (Fig. 2(a)). In contrast to this, when 10 mol.% $B_2O_3$ was incorporated into HAp powder, the diffraction intensity for HAp increased with increasing temperature to 1200 °C whereas the diffraction intensity for HAp remained unchanged during cooling to 700 °C (Fig. 2(b)).

Interpreting the data shown in Fig. 2, the authors suggest that during heating of the HAp with $Na_2CO_3$ addition, partial fusion of $Na_2CO_3$ (melting point, 859 °C) may have occurred prior to the thermal decomposition of $Na_2CO_3$ to $Na_2O$ (approximately 1000 °C). The chemical composition of the fused materials was suggested to have changed from $Na_2CO_3$ to $Na_2O$ with increasing temperature, judging from the fact that the melting point of $Na_2O$ is 1130 °C. The decrease in diffraction intensity of HAp may thus indicate the progressing reaction of HAp with the fused materials. In contrast to this, during the heating of HAp with $B_2O_3$ addition, the reaction of HAp and $B_2O_3$ appeared to occur at temperatures as low as 500 °C, presumably due to the low melting point (480 °C) of $B_2O_3$. Therefore, it is speculated that the reaction products formed on the surfaces of the HAp particles may have retarded mass transfer, resulting in the slow crystal growth of HAp, in addition to the delay in densification (see Fig. 1(c)).

On the basis of the above information, the authors investigated the effect of sintering temperature on the relative density and grain size of HAp ceramics with 10 mol.% $Na_2O$ or $B_2O_3$ addition. These sintered bodies were fabricated using pressureless sintering in the temperature range between 1000 and 1100 °C for 5 h with the results being shown in Fig. 3. The relative density of the HAp compact with 10 mol.% $Na_2O$ addition fired at 1000 °C for 5 h was 93.1% and this increased to 95.9% for temperatures up to 1100 °C. In addition, the grain size of the HAp compact with 10 mol.% $Na_2O$ addition increased with increasing firing temperature and attained 1.25 μm at the firing temperature of 1100 °C (Fig. 3(a)). In contrast to this, the relative density of the HAp compact with 10 mol.% $B_2O_3$ addition fired at 1000 °C for 5 h was 68.2% and this increased to 91.7% for temperatures up to 1100 °C. The grain size also increased with temperature, but still appeared to be submicrometer-sized (0.56 μm) at 1100 °C (Fig. 3(b)).

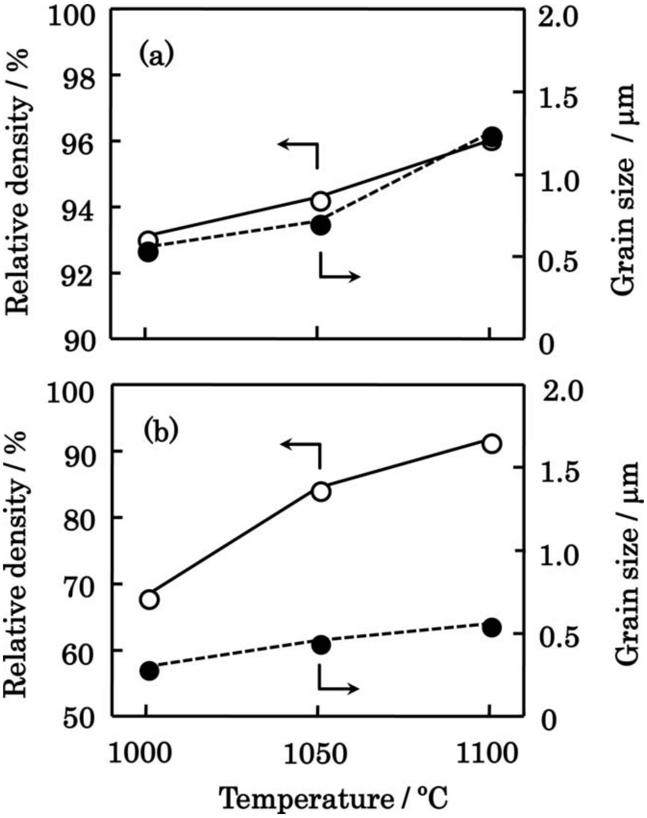

Fig. 3. Changes in relative density and grain size of HAp compacts with (a) 10 mol.% $Na_2O$ addition, and (b) 10 mol.% $B_2O_3$ addition pressuressly fired at each temperature for 5 h.

It is known that the liquid phase formed during sintering contributes to densification due to the rearrangement of grains. Simultaneously, the solution and precipitation mechanisms of grains may be repeatedly operated, thereby accelerating grain growth. Such mechanisms appear to predominantly operate for the case of $Na_2O$ addition over the case of $B_2O_3$ addition,[13] judging from the fact that the diffraction intensity of HAp was reduced with temperature above 900 °C. On the other hand, due to the melting point of $B_2O_3$ being as low as 480 °C, the fused materials reacted with HAp[14] to form products on the grain boundaries. In this case, it was believed that the fused materials did not contribute to either densification or mass transfer, due to their low formation temperature.

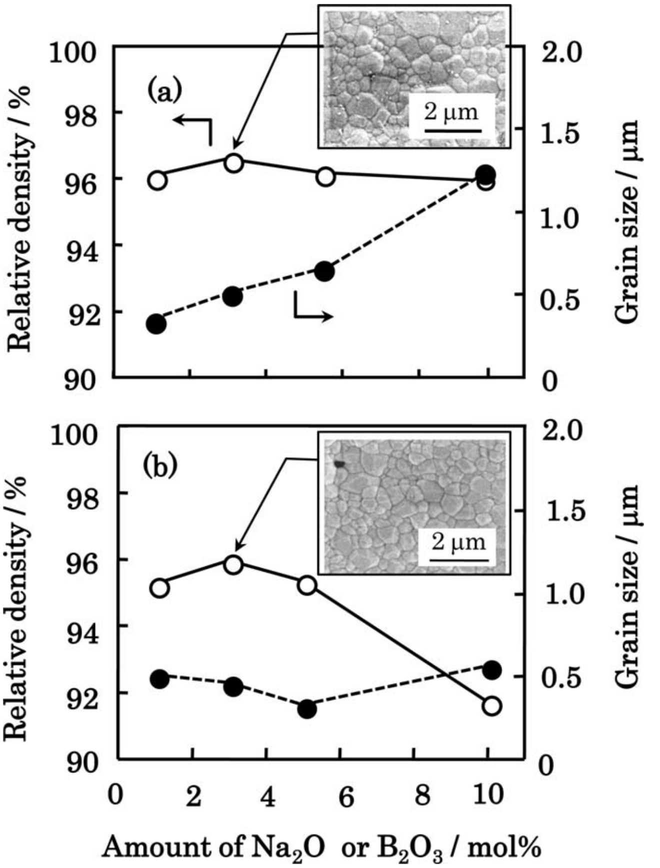

Fig. 4. Changes in relative density and grain size of HAp compacts with each additive amount of (a) $Na_2O$ and (b) $B_2O_3$ pressuressly sintered at 1100 °C for 5 h, together with typical FE-SEM micrographs.

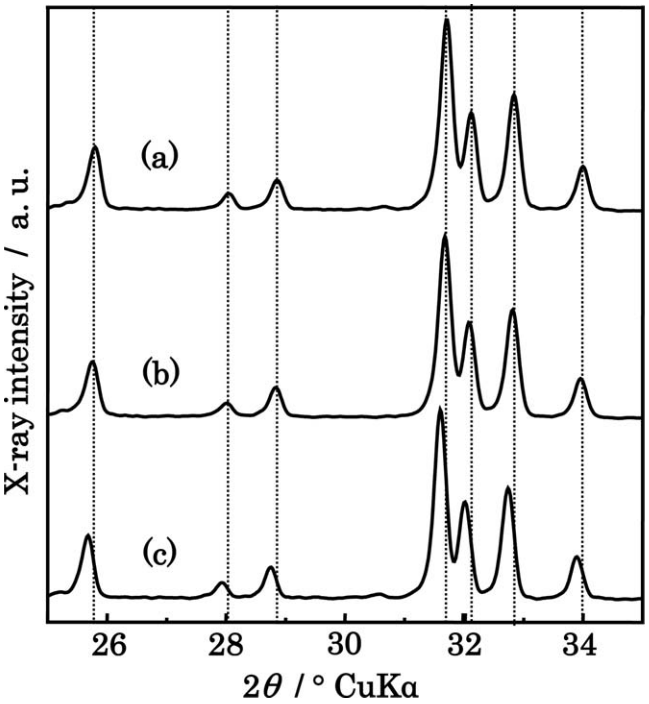

Fig. 5. XRD patterns of (a) pure HAp, (b) HAp with 3.0 mol.% $Na_2O$ addition, and (c) HAp with 3.0 mol.% $B_2O_3$ addition pressurelessly fired at 1100 °C for 5 h.

The authors further investigated the effect of the amount of $Na_2O$ or $B_2O_3$ addition on the relative density and grain size of HAp ceramic materials fabricated by pressureless sintering at a temperature between 1000 and 1100 °C for 5 h with the results being shown in Fig. 4, together with typical SEM micrographs. The maximum relative densities of the HAp ceramic materials were 96.6% for 3.0 mol.% $Na_2O$ addition and 96.0% for 3.0 mol.% $B_2O_3$ addition. Confirming such high relative densities, SEM micrographs showed the HAp ceramic materials with $Na_2O$ and $B_2O_3$ addition to be composed of closely packed grains. The grain sizes of the HAp ceramic materials measured using the intercept technique were 0.52 μm for 3.0 mol.% $Na_2O$ addition and 0.51 μm for 3.0 mol.% $B_2O_3$ addition. Whilst the grain sizes were similar for the case of 3.0 mol.% addition, the change in behavior for grain size was found to depend on the type of additive, *i.e.*, (i) an increase in grain size from 0.35 to1.25 μm ($Na_2O$ addition), and (ii) 0.33 to 0.56 μm ($B_2O_3$ addition), with increasing amount of $Na_2O$ or $B_2O_3$ addition from 1.0 to 10 mol.%.

The above results suggest that high-density HAp compacts containing 3.0 mol.% $Na_2O$ or $B_2O_3$ addition, *i.e.*, 96% or more, could be fabricated using pressureless sintering at 1100 °C for 10 min. Nevertheless, the grain growth mechanism for HAp compacts containing $Na_2O$ addition during pressureless sintering appears to be different from that of the HAp compact with $B_2O_3$ addition, *i.e.*, enhanced grain growth ($Na_2O$ addition) and restricted grain growth ($B_2O_3$ addition). On the basis of these results, the liquid phase in the $Na_2CO_3$–$Na_2O$ system was believed to contribute to grain growth on the basis of repeated solution–precipitation operations, whereas the $B_2O_3$-derived materials formed on the surfaces of grains and restricted mass transfer, thereby retarding grain growth.

Following this, crystalline phases present within the HAp compacts pressurelessly sintered at 1100 °C for 5 h were checked with the results being shown in Fig. 5, together with the case of the pressurelessly fired pure HAp compact. Note that the crystalline phases were examined following pulverization of the compacts. The only crystalline phase detected within the pulverized samples was HAp.[13] X-ray diffraction angles for the HAp powder with $Na_2O$ addition were almost in accordance with those of pure HAp powder (Fig. 5(a) and (b)). On the other hand, X-ray diffraction angles for the specimens containing $B_2O_3$ addition were shifted towards the lower-side when compared to the case of pure HAp powder (Fig. 5(c)). These results indicate that $Na_2O$ does not contribute to forming a solid solution but instead has the possibility of forming reaction products, whereas $B_2O_3$ has the possibility of forming a solid solution into the $Ca^{2+}$ sites for HAp. According to Ternane et al.,[15] $B_2O_3$ may be substituted for the $PO_4{}^{3-}$ and $OH^-$ sites in the HAp structure to form a compound with the following formula: $Ca_{10}\{(PO_4)_{6-x}(BO_3)_x\}\{(BO_3)_y(BO_2)_z(OH)_{2-3y-z}\}$. Such a compound may be present on grain boundaries and retard mass transfer with increasing thickness.

### *3.2. Properties of HAp compacts with $Na_2O$ or $B_2O_3$ addition fabricated by PCPS*

On the basis of the results shown in Section 3.1, the authors examined the fabrication conditions for high-density and submicrometer-sized HAp ceramic materials with $Na_2O$ or $B_2O_3$ addition using the pulse-current pressure sintering technique. Here, pulse-current pressure sintering enables the rapid sintering of powder compacts at relatively low temperature due to Joule heating generated through a pulsed electric current.[16,17] The firing of HAp compacts with $Na_2O$ or $B_2O_3$ addition using the PCPS technique was conducted at 1100 °C for 10 min; the amount of additive was fixed to be 3.0 mol.% as this amount was found to be optimum for achieving the highest density using standard pressureless sintering. Compounds in the $Na_2O$–$B_2O_3$ system are known to form a liquid phase at comparatively low temperatures and thus in this section the authors also examined the effect of an equimolar mixture of $Na_2O$ and $B_2O_3$ addition on densification and microstructure. The relative densities and grain sizes of HAp compacts with $Na_2O$ and $B_2O_3$ addition have been shown in Fig. 6. The relative densities of the sintered compacts were all 99.9%, except for the case of $B_2O_3$ addition (99.3%). On the other hand, the mean grain sizes of the sintered compacts varied significantly according to the type of additive: $Na_2O$ addition ($0.78\ \mu m$) > $B_2O_3$ addition ($0.51\ \mu m$) ≥ $B_2O_3$–$Na_2O$ addition ($0.49\ \mu m$) > no addition ($0.20\ \mu m$). As described previously, this arrangement may be explained in terms of the contribution of the liquid phase to promoting grain growth ($Na_2O$ addition) and that of secondary phases at the grain boundaries to the retardation of grain growth. Nevertheless, it should be noted that the mean grain size of the sintered HAp compact with $B_2O_3$ addition was larger than that of the sintered HAp compact with no addition. As described before, $B_2O_3$ may be substituted for the $PO_4{}^{3-}$ and $OH^-$ sites in the HAp structure to form the following compound: $Ca_{10}\{(PO_4)_{6-x}(BO_3)_x\}\{(BO_3)_y(BO_2)_z(OH)_{2-3y-z}\}$. The thickness of such a reaction phase may be reduced with increasing heating rate (25 °C min$^{-1}$, *i.e.*, short reaction time) and applied pressure (50 MPa, *i.e.*, the utilization of energy not only for diffusion but also for plastic deformation) during pulse current pressure sintering, which contribute to promoting mass transfer compared to the case of pressureless sintering.

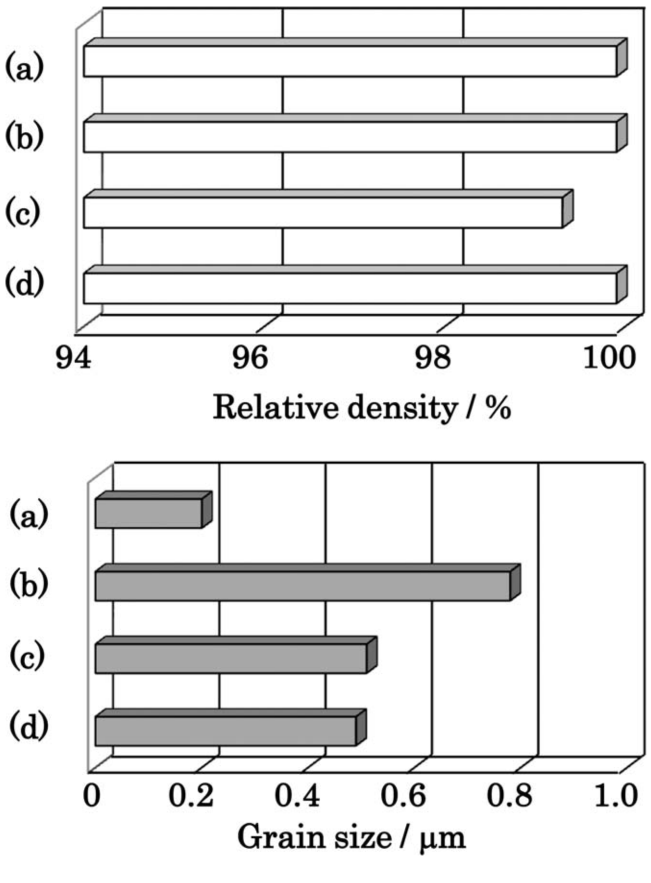

Fig. 6. Typical relative density and mean grain size of HAp compacts with (a) no addition, (b) HAp compact with 3.0 mol.% $Na_2O$ addition and (c) 3.0 mol.% $B_2O_3$ addition (d) 3.0 mol.% $B_2O_3$–$Na_2O$ addition ($B_2O_3/Na_2O = 1.0$) obtained using the PCPS technique at 1100 °C for 10 min under the pressure of 50 MPa.

Moreover, SEM micrographs of the microstructures and grain diameter distributions of the sintered compacts have been shown in Fig. 7. Note that the relative densities of these sintered compacts were all 99% or higher. The sintered HAp compact with 3.0 mol.% $Na_2O$ addition, which appeared to have a milky-white colored center and translucent outside, was composed of closely packed grains with diameters of 0.3–1.5 µm; the grain diameter distribution covered the range of 0.1–1.8 µm (Fig. 7(a)). The sintered HAp compact with 3.0 mol.% $B_2O_3$ addition, which appeared to possess a translucent body, was composed of closely packed grains with diameters of 0.1–1.0 µm; the grain diameter distribution was distributed over the range of 0.1–1.6 µm (Fig. 7(b)). Furthermore, the sintered HAp compact with 3.0 mol.% $B_2O_3$–$Na_2O$ addition ($B_2O_3/Na_2O = 1.0$), which appeared to posses an obscured translucency, was composed of closely packed grains with diameters of 0.1–1.0 µm; the grain diameters were distributed over the range of 0.1–1.2 µm (Fig. 7(c)). It should be noted that the grain size distribution for the sintered HAp compact appeared to be narrow, when compared to the case of $Na_2O$ addition, and that this mean grain size was larger than that of the pure HAp compact. This fact suggests that mass transfer may be promoted through the addition of $B_2O_3$.

Since high-density HAp ceramic materials with $Na_2O$ and/or $B_2O_3$ addition containing submicrometer-sized grains could be fabricated by pulse-current pressure sintering, the tensile strain for the HAp specimens was examined. High-temperature tensile tests examined at a test temperature of 1100 °C (tensile strain: $1.48 \times 10^{-4}\ s^{-1}$) have been shown in Fig. 8. The overall trend revealed that the true stress for the HAp specimens increased to a maximum value with increasing strain; this was followed by catastrophic fracture. The sintered HAp specimens with $Na_2O$ addition or with $Na_2O$–$B_2O_3$ addition fractured immediately following the increase in true stress; the tensile strains were 4.4% and 3.8%, respectively (Fig. 8(a) and (c)). In contrast to this, the true stress of the HAp specimen with $B_2O_3$ addition increased until the point of work hardening, after which the specimen broke, following the point of maximum stress; the tensile strain for this specimen was 139% (Fig. 8(b)).

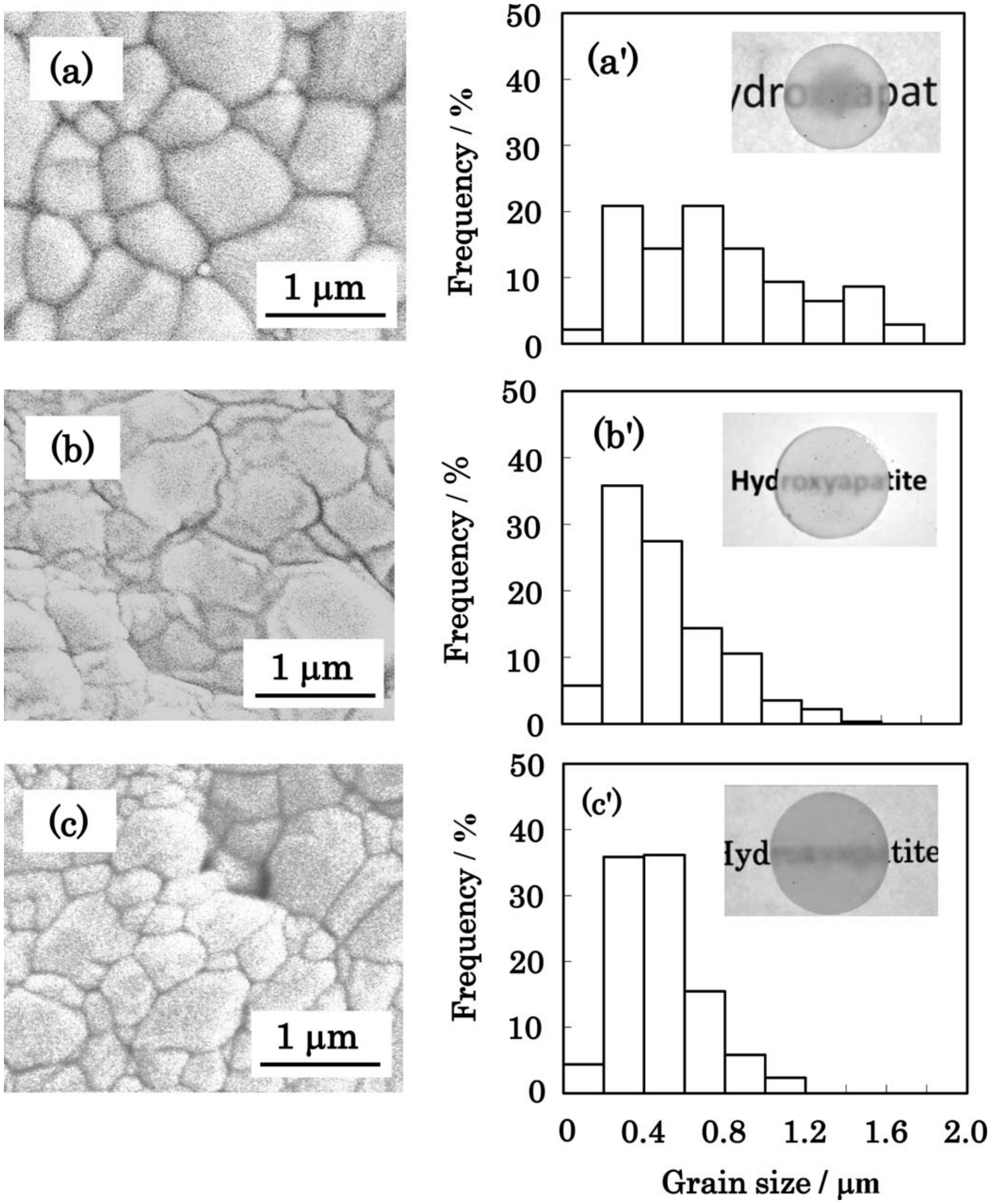

Fig. 7. FE-SEM micrographs and grain-size distributions of HAp compacts obtained by PCPS at 1100 °C for 10 min under a pressure of 50 MPa with (a) and (a′) 3.0 mol.% $Na_2O$ addition, (b) and (b′) 3.0 mol.% $B_2O_3$ addition, and (c) and (c′) 3.0 mol.% $B_2O_3$–$Na_2O$ addition ($B_2O_3/Na_2O = 1.0$).

From the above-mentioned results, no significant tensile strain was observed in the cases of sintered HAp specimens with $Na_2O$ addition. The probable premature breaking may be attributed to inoperative grain boundary sliding, based upon the phenomena of (i) the inhomogeneous presence of pores formed by the elimination of $CO_2$ due to the decomposition of $Na_2CO_3$ to $Na_2O$ during firing, and (ii) fusion at the local sites of the specimen during the test heating.

Grain growth during high temperature plastic deformation is known to cause the formation of cavities and microcracks. Therefore, control of grain growth during high temperature plastic strain is a vitally important problem. A higher tensile strain may be expected when the mean grain diameter of the specimen is kept at the micrometer level. On the basis of this information, the authors investigated the effect of firing temperature on the relative density and grain size of HAp ceramic materials with 3.0 mol.% $B_2O_3$ addition. These sintered bodies were fabricated by firing at a temperature between 1000 and 1100 °C for 10 min using PCPS with the results being shown in Fig. 9. The relative density of the HAp compact with 3.0 mol.% $B_2O_3$ addition fired at 1000 °C for 10 min was 98.8% and this increased to 99.3% with increasing temperature to 1100 °C. The grain size also increased with temperature but still appeared to be submicrometer-sized (0.51 μm) at a temperature of 1100 °C.

The high-temperature tensile testing of HAp specimens was examined at the same temperature as that of firing temperature through PCPS and at a tensile strain rate of $1.48 \times 10^{-4}\ s^{-1}$ with results being shown in Fig. 10. The tensile strain of the HAp specimens increased to a maximum value with increasing strain, followed by catastrophic fracture. The tensile strains

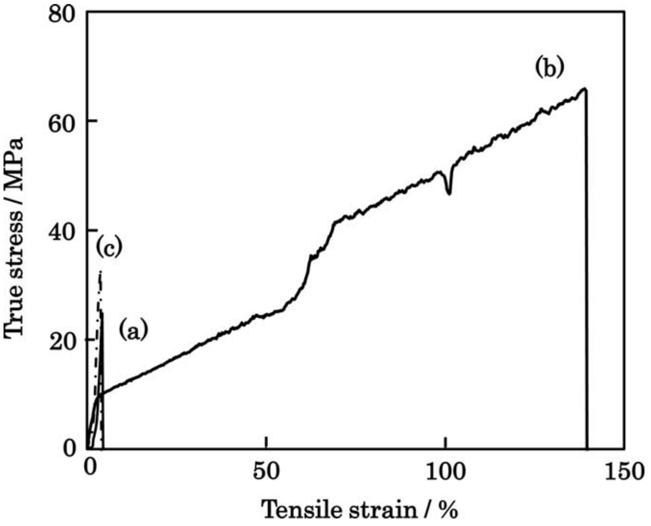

Fig. 8. Relationship between tensile strain and true stress of (a) HAp specimen with 3.0 mol.% $Na_2O$ addition, (b) HAp specimen with 3.0 mol.% $B_2O_3$ addition, (c) 3.0 mol.% $B_2O_3$–$Na_2O$ addition ($B_2O_3/Na_2O = 1.0$) by PCPS technique at 1100 °C for 10 min under a pressure of 50 MPa. Strain rate: $1.48 \times 10^{-4}$ s$^{-1}$. Test temperature: 1100 °C.

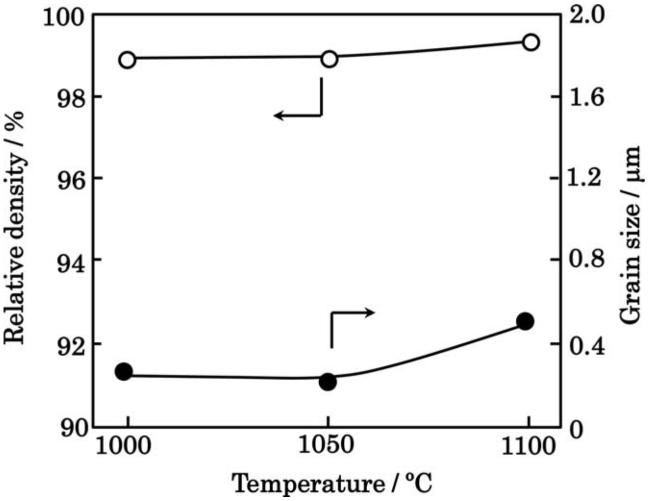

Fig. 9. Changes in relative density and grain size of HAp compacts with 3.0 mol.% $B_2O_3$ addition manufactured by PCPS at each temperature for 10 min under a pressure of 50 MPa.

of the sintered HAp compacts with $B_2O_3$ addition were clarified, according to the firing (=testing) temperature: 578% (1000 °C) > 391% (1050 °C) > 139% (1100 °C).

The tensile strain of the sintered HAp compact with $B_2O_3$ addition was thus enhanced as the firing/testing temperature became lower. The high tensile strain, *i.e.*, 578%, of the HAp specimen with $B_2O_3$ addition was thought to have most likely been achieved through efficient grain boundary sliding. Such efficient grain boundary sliding, as would be required for this relatively high tensile strain, suggests that the grain boundary was modified by the addition of $B_2O_3$, due to the formation of (amorphous) reaction products.

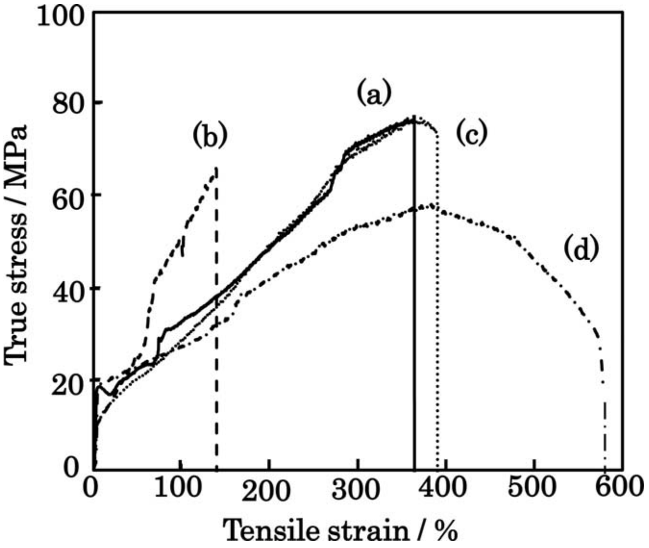

Fig. 10. Relationship between tensile strain and true stress of (a) HAp specimen manufactured by PCPS at 1100 °C for 10 min under a pressure of 50 MPa, and HAp specimens with 3.0 mol.% $B_2O_3$ addition manufactured by PCPS at (b) 1100 °C, (c) 1050 °C, (d) 1000 °C for 10 min under a pressure of 50 MPa. Strain rate: $1.48 \times 10^{-4}$ s$^{-1}$. Test temperature: same as sintered temperature.

## 4. Conclusions

The fabrication conditions for high-density HAp ceramic materials with $Na_2O$ and/or $B_2O_3$ addition containing submicrometer-sized grains were examined either by pressureless sintering or by pulse-current pressure sintering (PCPS). The results obtained were summarized as follows:

(i) HAp compacts with 1.0–10 mol.% $Na_2O$ and $B_2O_3$ addition were pressurelessly fired at a temperature between 1000 and 1100 °C for 5 h. The relative density and grain sizes of the HAp compacts with 3 mol.% $Na_2O$ addition were 91.7% and 0.56 μm, respectively, when the temperature increased to 1100 °C. On the other hand, the relative density and grain size of the HAp compact with 3.0 mol.% $B_2O_3$ addition were 95.9% and 1.25 μm, respectively, when the temperature increased to 1100 °C.

(ii) HAp compacts with 3 mol.% $Na_2O$ and/or $B_2O_3$ addition were pulse-current pressure sintered at 1100 °C for 10 min under a pressure of 50 MPa. The relative density of HAp compacts with $Na_2O$ addition, $B_2O_3$ addition and $B_2O_3$–$Na_2O$ addition ($B_2O_3/Na_2O = 1.0$) were all 99% or more. The grain sizes of these sintered compacts were on the micrometer level.

(iii) The tensile strain of the HAp specimen with 3 mol.% $B_2O_3$ addition pulse-current pressure sintered at 1000 °C for 10 min achieved 578% for a test temperature of 1000 °C and a strain rate of $1.48 \times 10^{-4}$ s$^{-1}$.

## References

1. Doremus RH, Bioceramics, review: bioceramics. *J Mater Sci* 1992;**27**:285–97.

2. Nishikawa M, Ohgushi H. Calcium phosphate ceramics in Japan. In: Yaszemski MJ, Trantolo DJ, Lewandrowski KU, Hasirci V, Altobelli DE, Wise DL, editors. *Biomaterials in orthopedics*. New York, NY: Marcel Dekker; 2004. p. 425–36.
3. Maehara Y, Langdon TG. Superplasticity in ceramics. *J Mater Sci* 1990;**25**:2275–86.
4. Wakai F. Dynamics of grain boundary network in ceramics superplasticity. *J Ceram Soc Jpn* 2004;**112**:472–6.
5. Sakka Y, Hiraga K. Preparation methods and superplastic properties of fine-grained zirconia and alumina based ceramics. *Nippon Kagaku Kaishi* 1999:497–508.
6. Sakka Y, Suzuki TS, Morita K, Nakano K, Hiraga K. Colloidal processing and superplastic properties of zirconia- and alumina-based nanocomposites. *Scripta Mater* 2001;**44**:2075–8.
7. Hiraga K, Kim BN, Morita K, Suzuki TS, Sakka Y. Microstructural design for high-strain-rate superplastic oxide ceramics. *J Ceram Soc Jpn* 2005;**113**:191–7.
8. Wakai F, Kodama Y, Sakaguchi S, Nonami T. Superplasticity of hot isostatically pressed hydroxyapatite. *J Am Ceram Soc* 1990;**73**:457–60.
9. Tago K, Itatani K, Suzuki TS, Sakka Y, Koda S. Densification and superplasticity of hydroxyapatite ceramics. *J Ceram Soc Jpn* 2005;**113**: 669–73.
10. Itatani K, Kobayashi A, Watanabe D, Davies IJ, Koda S. Superplasticity of hydroxyapatite specimen fabricated by two-step sintering. *J Inorg Mater Jpn* 2009;**16**:8–14.
11. Itatani K, Tago K, Nishio K, Sakka Y, Suzuki TS, Koda S.*Abstract of the annual meeting of the society of inorganic materials*. 2007. p. 8–9.
12. Morey GW, Merwin HE. Phase equilibrium relationships in the binary system, sodium oxide–boric oxide, with some measurements of the optical properties of the glasses. *J Am Chem Soc* 1936;**58**:2248.
13. Kalita SJ, Bose S, Hosick HL, Bandyopadhyay A. CaO–$P_2O_5$–$Na_2O$-based sintering additives for hydroxyapatite (HAp) ceramics. *Biomaterials* 2004;**25**:2331–9.
14. Saranti A, Koutselas IM, Karakassides A. Bioactive glasses in the system CaO–$B_2O_3$–$P_2O_5$: preparation, structural study and in vitro evaluation. *J Non-Cryst Solids* 2006;**352**:390–8.
15. Ternane R, Cohen-Adad MTh, Panczer G, Goutaudier C, Kbir-Ariguib N, Trabelsi-Ayedi M, Florian P, Massiot D. Introduction of boron in hydroxyapatite: synthesis and structural characterization. *J Alloys Comp* 2002;**333**:62–71.
16. Murayama N, Shin W. Effect of rapid heating on densification and grain growth in hot pressed alumina. *J Ceram Soc Jpn* 2000;**108**:799–802.
17. Tamari N, Tanaka T, Tanaka K, Kondoh I, Kawahara M, Tokota M. Effect of spark plasma sintering on densification and mechanical properties of silicon carbide. *J Ceram Soc Jpn* 1995;**103**:740–2.